Int. J. New. Chem., 2024, Vol. 11, Issue 4, pp. 424-442.

International Journal of New Chemistry

Published online 2024 in http://www.ijnc.ir/.

Open Access

Print ISSN: 2645-7236

Online ISSN: 2383-188x

Original Research Article

Boron Nitride Nanocluster ($B_{12}N_{12}$) Interaction with Nimorazole: A Comprehensive Theoretical Investigation

***Pedram Niknam Rad*[1], *Fatemeh Ashtari Mahini*[2,*]**

[1]*Department of Chemistry, Faculty of Science Hamedan Branch, Islamic Azad University, Hamedan, Iran*

[2] *Department of organic chemistry, Faculty of pharmaceutical chemistry, Tehran Medical Sciences, Islamic Azad University, Tehran, Iran*

*Corresponding author email address: f.ashtarimahini@gmail.com

Received: 2024-03-04 *Accepted: 2024-05-09* *Published: 2024-05-24*

ABSTRACT

The study focused on exploring the potential of pristine boron nitride nanocluster ($B_{12}N_{12}$) as an effective adsorbent and sensing material for the removal and detection of Nimorazole (NM). Through density functional theory simulations, the research revealed promising findings indicating that the interaction between NM and $B_{12}N_{12}$ is not only experimentally feasible but also exothermic and spontaneous. Additionally, the influence of solvent, particularly water, was investigated, with results demonstrating that the presence of water does not significantly impact these interactions. Furthermore, the impact of temperature on the thermodynamic parameters was considered, with results indicating that the adsorption process is more favorable at lower temperatures. The study also utilized frontier molecular orbital calculations, which revealed a substantial change in the bandgap of $B_{12}N_{12}$ during the adsorption process of NM. Specifically, the bandgap was found to increase by 70.795%, from 6.716 (eV) to 11.470 (eV), indicating significant alterations in the electronic properties of $B_{12}N_{12}$ upon interaction with NM. Moreover, the investigation included Quantum Theory of Atoms in Molecules (QTAIM) and Natural Bond Orbital (NBO) studies, which provided insights into the nature of these interactions, indicating a physisorption nature. Overall, the theoretical findings strongly suggest that $B_{12}N_{12}$ has the potential to serve as an excellent adsorbent and sensor for the removal and detection of NM. This research contributes valuable knowledge to the field of nanomaterials and offers a promising direction for the development of effective strategies for addressing the challenges associated with NM removal and detection.

Keywords: Nimorazole, Density functional theory, Adsorption, Sensor, Removal

Introduction

The increasing use of antibiotics in the treatment and prevention of bacterial infections has led to a concerning environmental issue – their presence in the aquatic environment [1]. This problem is primarily attributed to the discharge of effluents from pharmaceutical industries, hospitals, as well as the use of veterinary and human medications [2]. The widespread application of antibiotics has undoubtedly brought about significant advancements in healthcare by effectively combating bacterial infections [3]. However, the unintended consequence of their presence in the aquatic environment poses a threat to ecosystems and human health [4]. The discharge of antibiotics into water bodies can eventuate to the development of antibiotic-resistant bacteria, also known as superbugs [5]. These superbugs can spread through water systems and pose a serious risk to public health as they can cause infections that are resistant to common antibiotic treatments [6]. Furthermore, exposure of antibiotics to the environment can disrupt the natural balance of microbial communities [7]. This disruption can have far-reaching effects on the ecosystem, including impacts on nutrient cycling, food webs, and overall ecosystem health [8]. In addition to the environmental implications, the presence of antibiotics in water bodies can also have direct consequences for aquatic organisms [9]. Studies have shown that exposure to antibiotics can negatively impact the growth, reproduction, and survival of various aquatic species, including fish and invertebrates [10]. Nimorazole (NM) is indeed a nitroimidazole antibiotic that has been widely prescribed for a variety of infections [11]. Its mechanism of action involves targeting and inhibiting the growth of certain bacteria and parasites, making it effective in treating conditions such as trichomoniasis, giardiasis, and amoebiasis [12]. Additionally, NM has shown promise in the treatment of certain types of cancer, particularly head and neck cancers [13]. As an antibiotic, NM works by disrupting the DNA synthesis of microorganisms, ultimately leading to their death [14]. This makes it a valuable tool in combating infections caused by anaerobic bacteria and protozoa [15]. Its broad spectrum of activity allows for its use in treating a range of infections, from mild to severe [16]. The identification and elimination of NM in environmental samples is crucial due to its role as an antibiotic medication [17]. Additionally, the search for a nanocarrier for targeted drug delivery of NM is of considerable importance in the field of anticancer research [18]. Both aspects highlight the significance of addressing NM in various contexts, from environmental impact to potential therapeutic applications [19]. This underscores the need for continued research and development

in the detection, removal, and targeted delivery of NM, contributing to advancements in both environmental and medical sciences [20].

The research on boron nitride nanocage ($B_{12}N_{12}$) has revealed its potential as a versatile material with various applications in the field of wide-gap semiconductors [21]. This nanocage has been found to possess several desirable chemical and physical characteristics, making it an ideal candidate for addressing environmental and analytical challenges [22]. Studies have shown that $B_{12}N_{12}$ is renowned for its outstanding attributes, such as a low dielectric constant, high thermal conductivity, exceptional structural and thermal stability, specific surface area ratio, wide bandgap, and superb oxidation resistance [23]. These features establish it as an extremely sought-after material for a range of uses in electronics, thermal management, and structural purposes [24]. Furthermore, the stability, geometry, and properties of boron nitride fullerenes, particularly $B_{12}N_{12}$, have been extensively evaluated. Among various (BN)n nanoclusters, $B_{12}N_{12}$ has emerged as the most stable cluster [25]. This stability further enhances its suitability for applications such as environmental remediation and analytical sensing. Several investigations have explored the adsorption of different species on the surface of $B_{12}N_{12}$, including H_2S, quetiapine, and Norfloxacin [26-28]. These studies have highlighted the potential of boron nitride nanocage in addressing environmental and analytical challenges, further supporting its utility in diverse applications [29, 30]. The current study aims to investigate the adsorption of NM on the surface of BN nanocage and assess the impact of various parameters such as the presence of solvent and temperature on their interactions. To achieve this, the research utilizes IR, NBO, QTAIM, and FMO computations to analyze the interactions. The insights gained from this analysis will provide valuable information regarding the potential applications of $B_{12}N_{12}$ as an adsorbent, sensing material, and nanocarrier for the detection, removal, and drug delivery of NM.

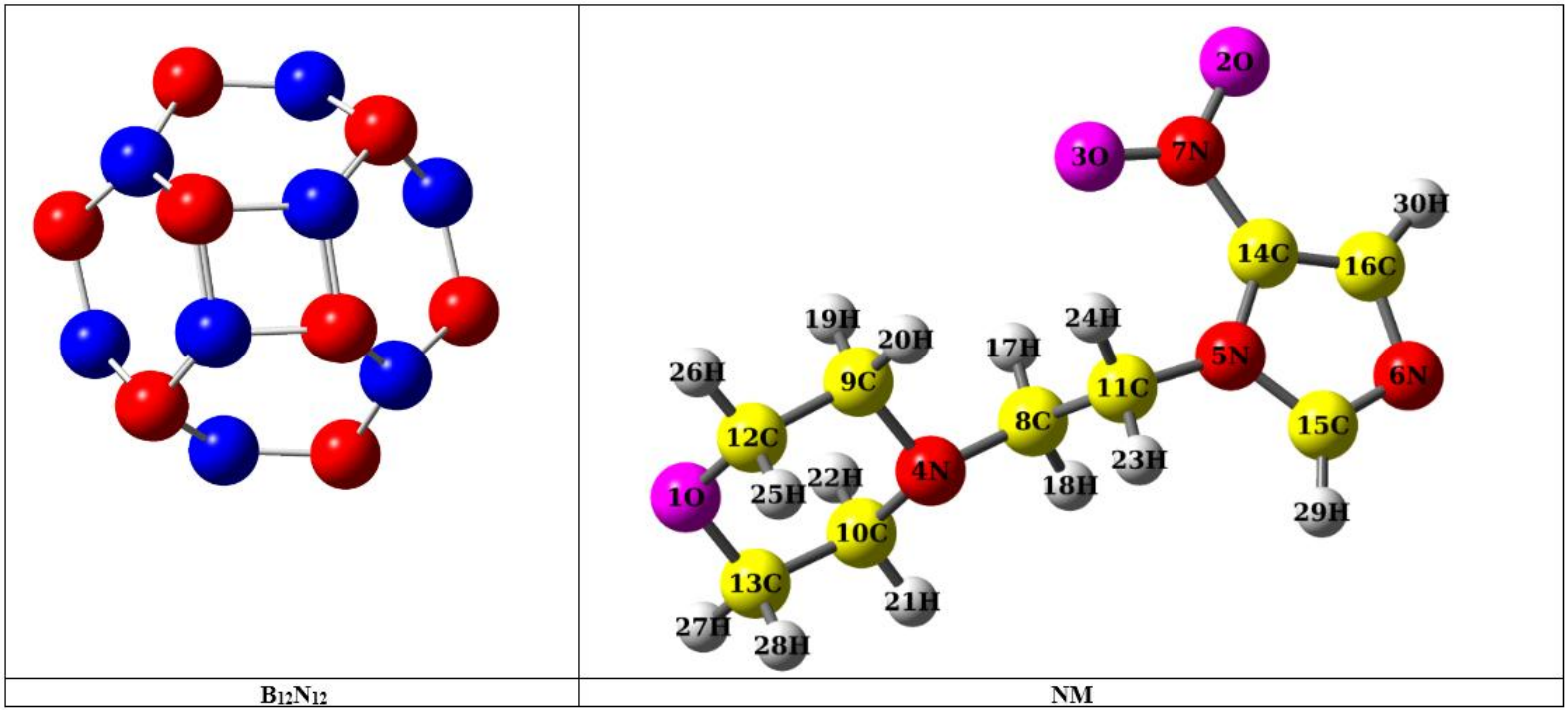

Fig. 1. Optimized structures of NM and $B_{12}N_{12}$

Computational Details

We utilized GuassView 6 [31] and Nanotube Modeler 1.3.0.3 [32] software versions for designing the $B_{12}N_{12}$, NM, and their complexes. After the design phase, we performed geometric optimization for each structure. Subsequently, we conducted various computations including infra-red (IR), frontier molecular orbital (FMO), natural bond orbital (NBO) and quantum theory of atoms in molecules (QTAIM) on the optimized structures. The density functional theory (DFT) method, specifically the B3LYP/6-31G (d) level of theory, was consistently applied using Gaussian 16 [33] software version. The selection of this level of theory was based on its prior acceptance and consistency with experimental findings. It has been widely used in the scientific community due to its proven reliability in predicting experimental results. This decision was made to ensure that the theoretical calculations closely match the actual observations, thereby enhancing the validity and applicability of the research findings. [26-30]. The DOS spectra were obtained using GaussianSum 3.0 software [34] for analyzing electronic structure, while QTAIM computations were done with AIM 2000 [35]. The study conducted computations in both

vacuum and aqueous phases using the CPCM [36] solvation method. Temperatures ranging from 298 K to 398 K were investigated, focusing on drug adsorption onto an adsorbent material. The aim was to understand how solvation and temperature influence the process, specifically in aqueous environments. This approach provides insights into the thermodynamics of drug adsorption and could contribute to improving drug delivery systems in water-based settings [37].

Drug + Adsorbent → Drug-Adsorbent (1)

To evaluate the strength of the drug-adsorbent interaction, adsorption energy values (E_{ad}) and various thermodynamic parameters were calculated. These thermodynamic parameters include the thermodynamic equilibrium constant (K_{th}), entropy changes (ΔS_{ad}), Gibbs free energy changes (ΔG_{ad}), and adsorption enthalpy changes (ΔH_{ad}). The calculations of these parameters were carried out using equations 2–6 [38].

$$E_{ad} = \left(E_{(Complex)} - \left(E_{(Drug)} + E_{(Adsorbent)+}E_{(BSSE)}\right)\right) \quad (2)$$

$$\Delta H_{ad} = \left(H_{(Complex)} - \left(H_{(Drug)} + H_{(Adsorbent)}\right)\right) \quad (3)$$

$$\Delta G_{ad} = \left(G_{(Complex)} - \left(G_{(Drug)} + G_{(Adsorebnt)}\right)\right) \quad (4)$$

$$\Delta S_{ad} = \left(S_{(Complex)} - \left(H_{(Drug)} + H_{(Adsorbent)}\right)\right) \quad (5)$$

$$K_{th} = \left(exp - (\Delta G_{ad}/RT)\right) \quad (6)$$

Overall, the software tools and computational methods employed in this study allowed for the design and analysis of various structures and their complexes. The investigation focused on understanding the drug-adsorbent interaction through the calculation of adsorption energy values and thermodynamic parameters. The results obtained from these calculations will contribute to a better understanding of the adsorption process and provide valuable insights for future drug design and development efforts. "In the aforementioned equations, the variable E represents the total electronic energy for each structure being studied. E_{BSSE}, on the other hand, denotes the basis set superposition correction. The variable H encompasses the total energy of the evaluated

materials along with the thermal correction of enthalpy. Similarly, G symbolizes the total energy plus the thermal correction of the Gibbs free energy, as described in reference. R refers to the constant of the ideal gas, while S represents the thermal correction entropy for the structures under investigation. Lastly, T corresponds to the temperature, as outlined in reference [39-41].

These equations, specifically equations 7–12, are utilized for the computation of several crucial properties. The bandgap (Eg), chemical hardness (η), chemical potential (μ), maximum charge capacity (ΔN_{max}), and electrophilicity (ω) of frontier molecular orbitals are all calculated using these equations [42].

$$E_g = E_{LUMO} - E_{HOMO} \quad (7)$$

$$\%\Delta E_g = \frac{E_{g2} - E_{g1}}{Eg1} \times 100 \quad (8)$$

$$\eta = {(E_{LUMO} - E_{HOMO})}/{2} \quad (9)$$

$$\mu = {(E_{LUMO} + E_{HOMO})}/{2} \quad (10)$$

$$\omega = {\mu^2}/{2\eta} \quad (11)$$

$$\Delta N_{max} = -{\mu}/{\eta} \quad (12)$$

In the given equations, E_{LUMO} represents the energy of the lowest unoccupied molecular orbital, while E_{HOMO} represents the energy of the highest occupied molecular orbital. The bandgaps of the Nano-adsorbent and NM-Adsorbent complexes are denoted as Eg_1 and Eg_2, respectively [42].

Results and discussion

Structural Analysis

The analysis of the initial and optimized structures of NM-$B_{12}N_{12}$ complexes, as depicted in Figure 2, reveals the investigation of interactions at two distinct configurations to ascertain the most stable conformer. In the A-Conformer, the nitro group of NM is positioned in a parallel

orientation towards the BN nanocage, while in the B-Conformer, the adsorbent is situated in close proximity to the morpholine ring of NM in a parallel fashion. The total electronic energy values of both conformers are presented in Table 1, indicating that the total electronic energy of the A-Conformer is lower than that of the B-Conformer in both vacuum and aqueous phases. This suggests that the formation of the A-Conformer is more energetically favorable than the B-Conformer [43]. Furthermore, the calculated adsorption energies, also tabulated in Table 1, demonstrate negative values, signifying that the interaction of NM with $B_{12}N_{12}$ is experimentally feasible, and the presence of water as a solvent does not significantly impact the interactions [44]. Additionally, the calculated IR frequencies provided in Table 1 reveal that no negative frequency was obtained, implying that all scrutinized structures represent true local minimums [45].

Moreover, the dipole moment of NM was approximately 2.9 (Debye), but post-interaction with the BN nanocage, this parameter significantly increased [46]. This enhancement suggests that NM-$B_{12}N_{12}$ complexes exhibit improved solubility in polar solvents and enhanced biocompatibility of NM after adsorption on the nano-adsorbent. These findings contribute to a deeper understanding of the behavior and properties of NM-$B_{12}N_{12}$ complexes, shedding light on their potential applications and implications in various fields [47].

Table 1. The calculated values of total electronic energy, adsorption energy, zero-point energy (ZPE), maximum and minimum IR frequency, and dipole moment

	Total electronic energy (a.u)	Adsorption energy (kJ/mol)	Zero-point energy (kJ/mol)	Minimum IR frequency (cm^{-1})	Mazimum IR frequency (cm^{-1})	Dipole moment (Debye)
NM (Vacuum)	-781.169	---	752.292	21.540	3770.820	2.820
NM (Water)	-781.174	---	749.910	19.980	3772.780	2.940
$B_{12}N_{12}$ (Vacuum)	-938.543	---	391.643	369.810	1653.630	0.000
$B_{12}N_{12}$ (Water)	-938.546	---	401.109	371.190	1649.980	0.010
A-Conformer (Vacuum)	-1719.781	-181.160	1150.142	8.480	3759.370	10.470
A-Conformer (Water)	-1719.766	-121.823	1169.710	9.980	3760.110	9.870
B-Conformer (Vacuum)	-1719.773	-160.156	1322.780	13.190	3769.880	3.980
B-Conformer (Water)	-1719.761	-108.696	1327.810	14.110	3770.820	4.510

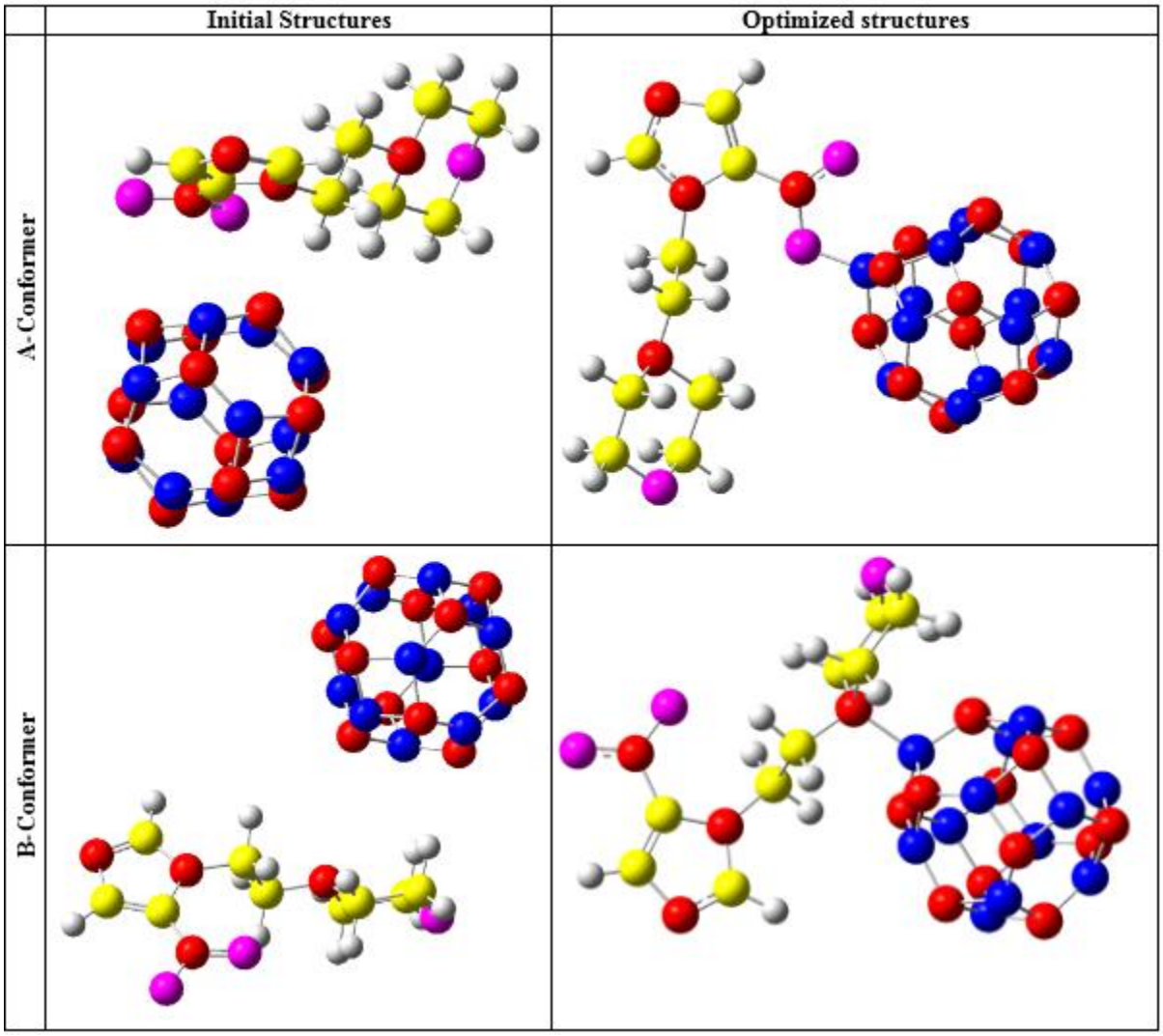

Fig. 2. The initial and optimized structures of NM-$B_{12}N_{12}$ complexes

Thermodynamic parameters

The calculated values of ΔH_{ad}, ΔG_{ad}, K_{th}, and ΔS_{ad} as a function of temperature are depicted in figures 3-6, respectively. The findings reveal that the interaction of NM with $B_{12}N_{12}$ is characterized by spontaneity, exothermicity, two-sidedness, and thermodynamic feasibility. This is supported by the negative values of ΔH_{ad} and ΔG_{ad}, as well as the negligible values of K_{th} observed for both conformers [48]. Interestingly, the presence of water as the solvent did not exert a significant influence on these thermodynamic parameters. Furthermore, the influence of temperature on the adsorption process was evaluated, indicating that the interactions are more

favorable at lower temperatures [43]. Notably, the negative values of ΔS_{ad} suggest that the adsorption process is unfavorable in terms of entropy, signifying a decrease in chaos during the interactions [44]. This phenomenon may be attributed to the aggregation that occurs during the formation of complexes [45].

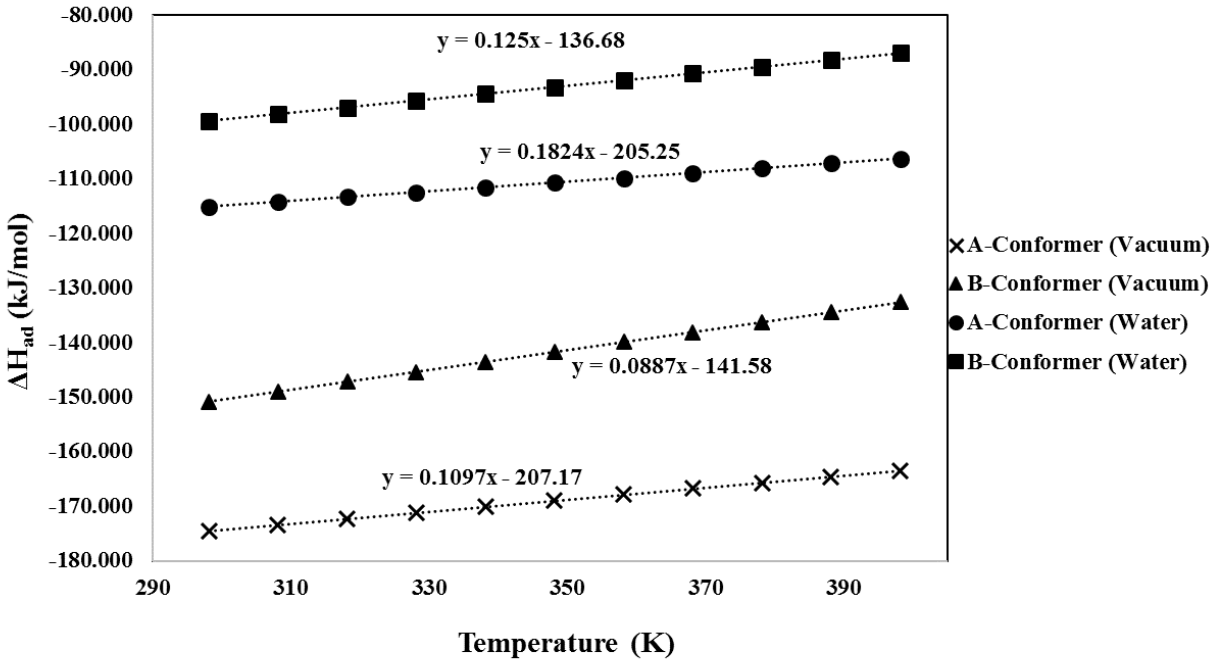

Fig. 3. ΔH_{ad} values as a function of temperature in the range of 298-398 K at 10° intervals in both vacuum and aqueous phases

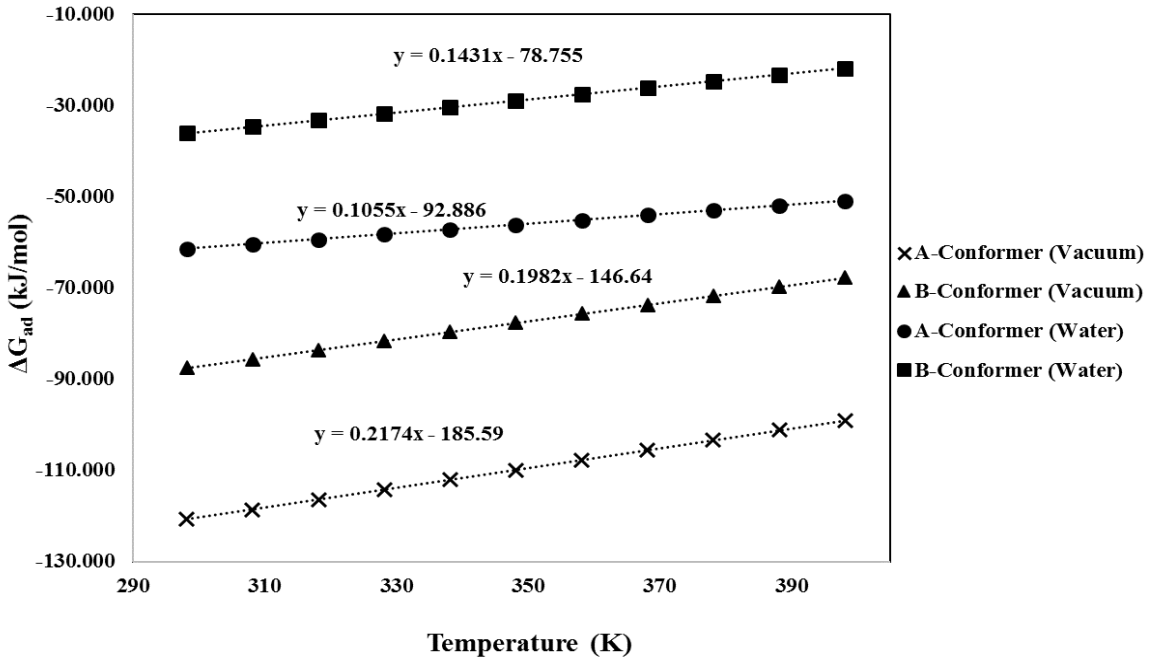

Fig. 4. ΔG_{ad} values as a function of temperature in the range of 298-398 K at 10° intervals in both vacuum and aqueous phases

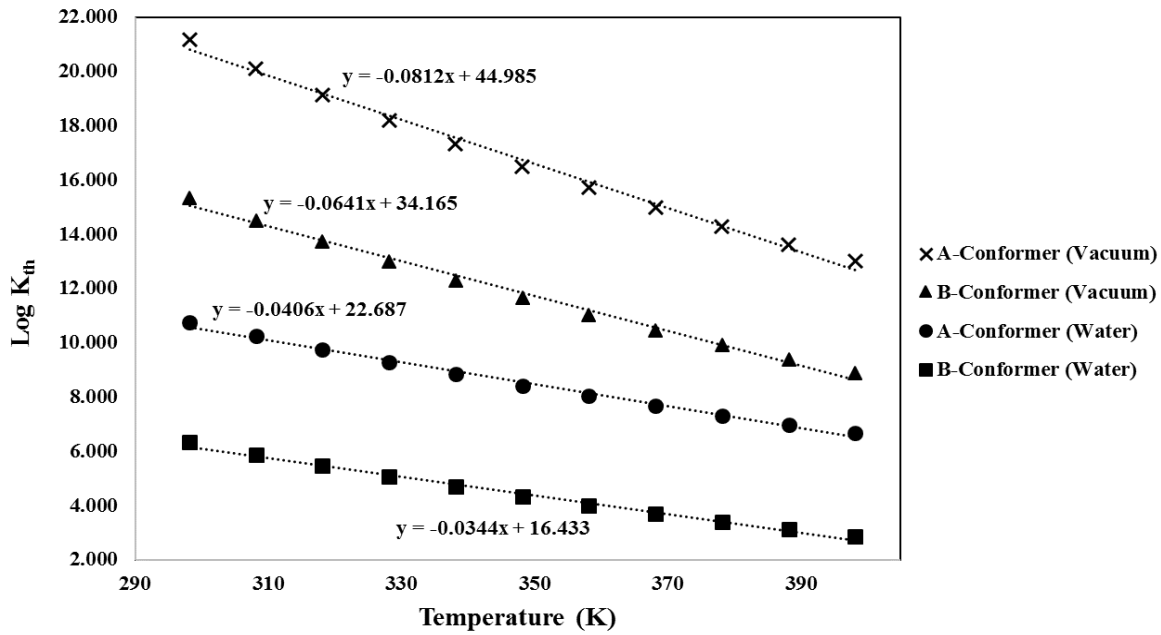

Fig. 5. Log K_{th} values as a function of temperature in the range of 298-398 K at 10° intervals in both vacuum and aqueous phases

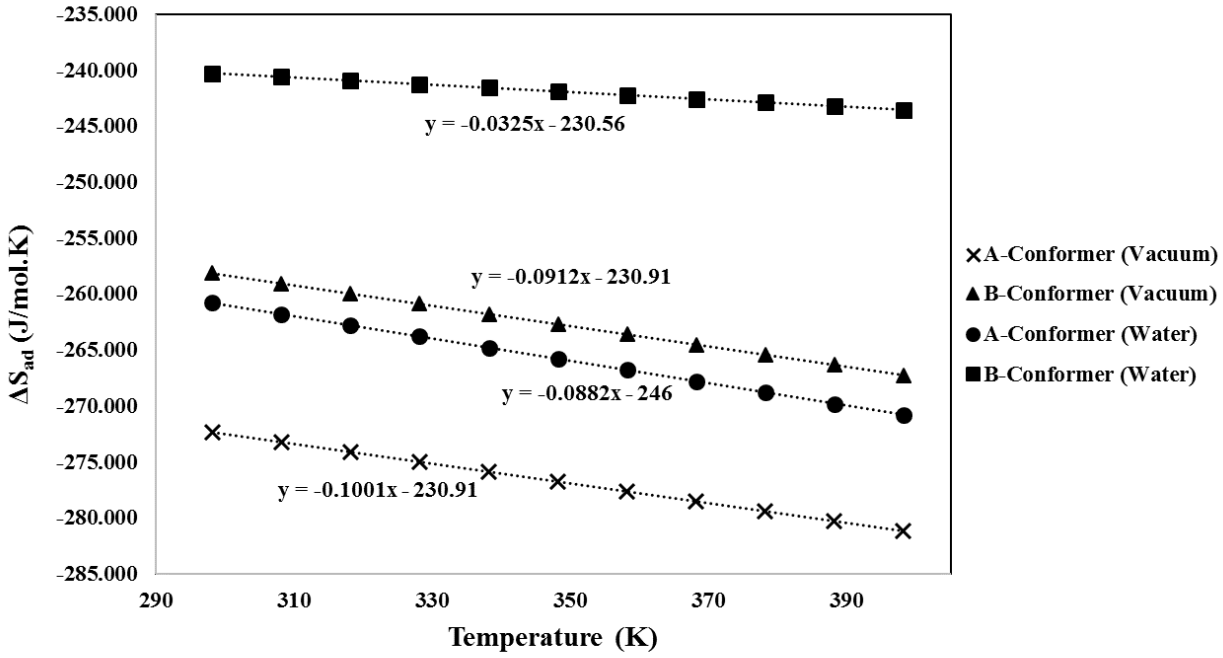

Fig. 6. ΔS_{ad} values as a function of temperature in the range of 298-398 K at 10° intervals in both vacuum and aqueous phases

QTAIM and NBO Studies

As the presented data in Fig. 7 show chlearly, at A and B conformers 3 and 4 bond critcal points (BCPs) have been observed after geometrical optimizations berween NM and the adsorbent. The relevant data to these BCPs are given in Table 3. As can be observed, the values of $G \div \nu(-1)$ are bigger than 1 which implies the BCPs have a non-covalent nature except the O_3…B and N_4…B BCPs in A and B conformers because $G \div \nu(-1)$ values are 0.869 and 0.680 indicating the partly covalent nature of the BCPs [46]. Furthermore, the NBO results of the same BCPs that are given in Table 4 also confirms the aforementioned results because the values of E(2) are low in most

BCPs but in the cases of O_3…B and N_4…B this parameter increased significantly indicating more energy is required for the breaking of those bonds in comparison to others [47, 48].

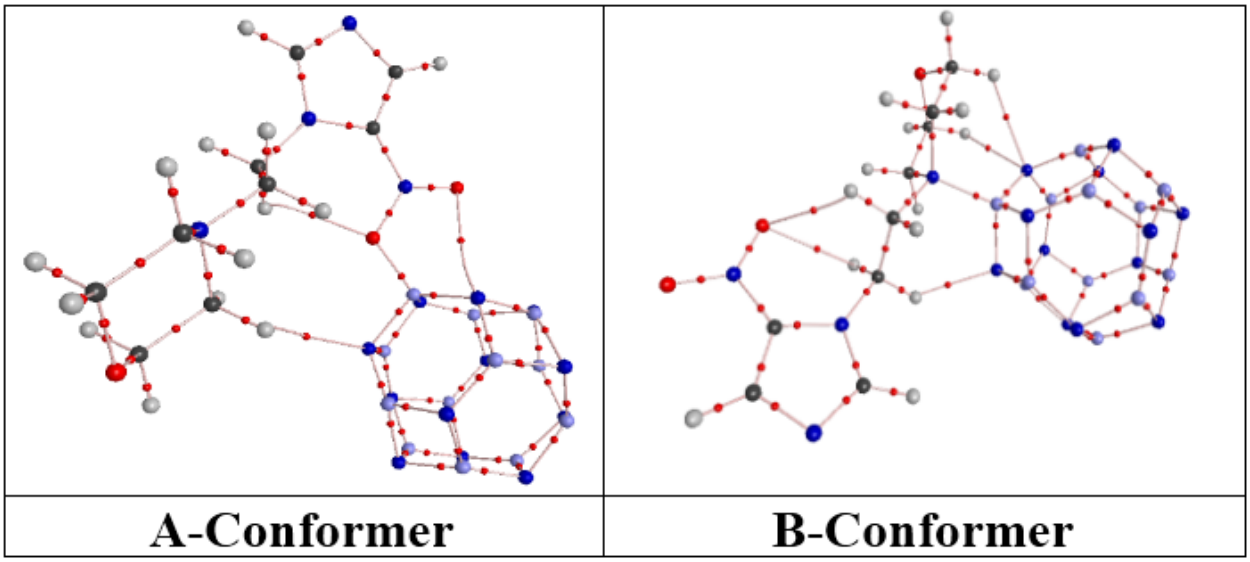

Fig. 7. The BCPs between NM and BN nanocage

Table 3. BCPs data (in a.u.) from QTAIM in molecular analysis

	BCPs	Rho(r)	∇ρ	G(r)	H(r)	v(r)	E(A…B)=v/2	G ÷ v(–1)	bond type
A-Conformer	H19….N	0.002	0.009	0.002	0.001	-0.001	-0.317	1.632	non-covalent
	O3…B	0.100	0.697	0.205	-0.031	-0.236	-74.153	0.869	partly covalent
	O2.. .N	0.014	0.071	0.016	0.001	-0.015	-4.717	1.093	non-covalent,
B-Conformer	H23…N	0.020	0.092	0.020	0.003	-0.017	-5.350	1.173	non-covalent
	N4…B	0.101	0.269	0.127	-0.060	-0.187	-58.654	0.680	partly covalent
	H25…N	0.011	0.059	0.012	0.003	-0.009	-2.735	1.345	non-covalent
	H28…N	0.010	0.052	0.010	0.003	-0.007	-2.347	1.373	non-covalent

Table 4. NBO analysis of BCPs

	BCPs	Donor NBO (i)	Acceptor NBO (j)	E(2) kcal/mol
A-Conformer	H19….N	126. LP (1) N 4	/330. BD*(1) C 9 - H 19	0.800
	O3…B	(1) O 3	/133. LP*(1) B 50	4.5
	O2….. .N	(1) N 45	/314. BD*(1) O 3 - B 50	0.440
B-Conformer	H23……N	56. BD (1) N 38 - B 44	/332. BD*(1) C 11 - H 23	0.560
	N4……B	86. CR (1) N 4	/245. RY*(3) B 39	2.08
	H25……N	50. BD (2) N 35 - B 40	/334. BD*(1) C 12 - H 25	1.75

		50. BD (2) N 35 - B 40	/334. BD*(1) C 12 - H 25	1.75
	H28……N	50. BD (2) N 35 - B 40	/337. BD*(1) C 13 - H 28	1.61
		49. BD (1) N 35 - B 40	/337. BD*(1) C 13 - H 28	0.59

FMO Analysis

The DOS spectra of $B_{12}N_{12}$ and its complexes with NM are presented in Figure 8. It can be observed that the bandgap of BN nanocage is 6.716 eV. However, when NM is adsorbed on its surface, the bandgap increases to 8.496 eV, and 11.470 eV in A, and B conformers respectively, representing an incrementing of approximately 26.514%, and 70.795%. The bandgap of a compound is inversely related to its electrochemical conductivity. A molecule with a narrow bandgap exhibits higher conductivity compared to a compound with a wider bandgap [43]. Therefore, significant changes in the bandgap can serve as an analytical signal for the detection of the desired analyte, in this case, NM. In this regard, $B_{12}N_{12}$ appears to be a suitable sensing material for the detection of NM as its bandgap gets wider significantly when NM adsorbs on $B_{12}N_{12}$ surface [44]. Additional molecular orbital parameters such as chemical potential, chemical hardness, electrophilicity, and maximum transferred charge were also calculated and are reported in Table 5. The negative values for the chemical potential indicate that all of the studied structures are thermodynamically stable [45]. The chemical hardness of NM is 6.037 eV, and when it interacts with $B_{12}N_{12}$, this parameter experiences a slight decrease in all of the complexes. Chemical hardness is inversely proportional to chemical reactivity, meaning that a compound with lower chemical hardness is more reactive than one with a higher value [46]. Therefore, it can be inferred that NM complexes with BN nanoclusters exhibit higher chemical reactivity compared to pure NM without any nanocage. The calculated values of electrophilicity and maximum transferred charge are also provided in Table 3. Both indices indicate the tendency of a molecule to absorb electrons. It is evident from the table that both indices for NM show a significant increase after interaction with BN nanocluster [47]. Thus, it can be concluded that NM complexes with $B_{12}N_{12}$ are more electrophilic than pure NM without any nanostructures. Overall, the analysis of the DOS spectra and molecular orbital parameters suggests that $B_{12}N_{12}$ nanoclusters has unique properties when interacting with NM, making them potential candidates for sensing applications or other relevant fields [48].

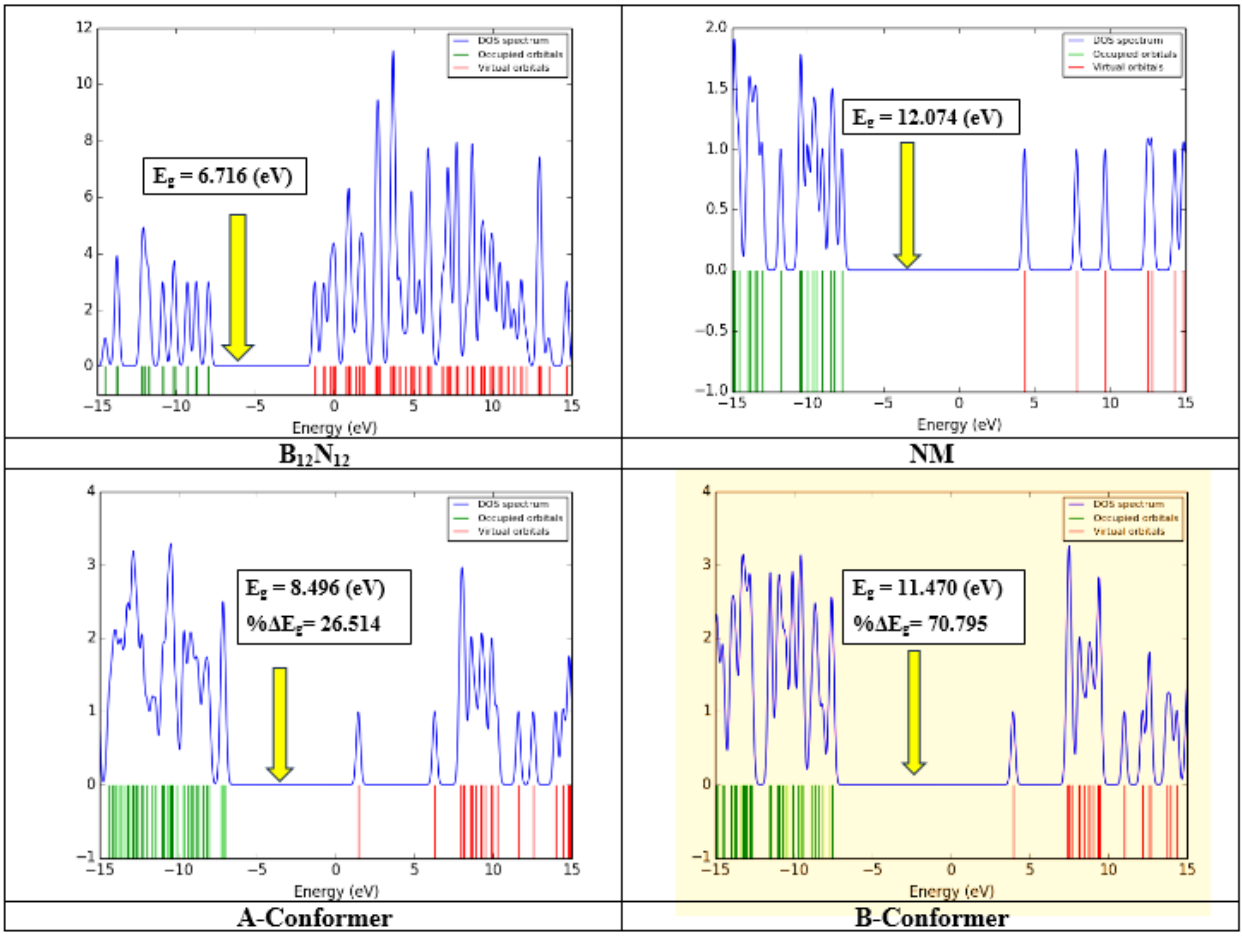

Fig. 8. DOS spectrums of $B_{12}N_{12}$, NM and their complexes

Table 5. The calculated FMO parameters for NM, $B_{12}N_{12}$, and their complexes

	E_{HOMO} (eV)	E_{LUMO} (eV)	Eg (eV)	%ΔEg	η (eV)	μ (eV)	ω (eV)	ΔN_{max} (eV)
NM	-7.732	4.343	12.074	---	6.037	-1.695	0.238	0.281
$B_{12}N_{12}$	-7.955	-1.239	6.716	---	3.358	-4.597	3.146	1.369
A-Conformer	-7.054	1.442	8.496	26.514	4.248	-2.806	0.927	0.661
B-Conformer	-7.531	3.939	11.470	70.795	5.735	-1.796	0.281	0.313

Conclusion

The study undertaken was focused on the exploration of the potential of pristine boron nitride nanocluster ($B_{12}N_{12}$) as an adsorbent and sensing material for the removal and detection of NM using density functional theory simulations. The results obtained from the simulations indicated

that the interaction between NM and $B_{12}N_{12}$ is not only feasible but also exothermic, suggesting spontaneity in the process. Furthermore, the impact of water as a solvent on these interactions was carefully examined, revealing that its presence has minimal effect on the adsorption and detection capabilities of $B_{12}N_{12}$. In addition, the study delved into assessing the influence of temperature on the thermodynamic aspects of the interactions. The findings showed that lower temperatures favor the adsorption process, providing valuable insights for potential practical applications. Moreover, frontier molecular orbital calculations revealed a significant change in the bandgap of $B_{12}N_{12}$ during the NM adsorption process, with the bandgap increasing by 70.795% from 6.716 (eV) to 11.470 (eV). This finding holds significant implications for the material's potential as an effective adsorbent and sensor for NM removal and detection. Furthermore, analysis through Quantum Theory of Atoms in Molecules (QTAIM) and Natural Bond Orbital (NBO) studies indicated that the interactions between B_{12}N12 and NM demonstrate physisorption characteristics. This understanding adds a layer of insight into the nature of the interactions, contributing to the comprehensive assessment of $B_{12}N_{12}$'s potential in addressing the crucial need for effective NM removal and detection. In conclusion, the theoretical findings derived from this study strongly imply that boron nitride nanocluster ($B_{12}N_{12}$) holds great promise as an effective adsorbent and sensor for the removal and detection of NM. The implications of this research are significant, as it highlights the promising application of $B_{12}N_{12}$ in addressing the critical need for advancements in NM removal and detection, thereby contributing to progress in this important area of study.

References

1. Z. Y. Lu, Y. L. Ma, J. T. Zhang, N. S. Fan, B. C. Huang, R. C. Jin, *J. Water. Process. Eng.*, *38*, 101681 (2020).
2. M. S. de Ilurdoz, J. J. Sadhwani, J. V. Reboso, J. Water. Process. Eng., 45, 102474 (2022).
3. Z. Derakhshan, M. Mokhtari, F.. Babaei, R. Malek Ahmadi, M. H. Ehrampoush, M. Faramarzian, *J. Environ. Health. Sustain. Develop.*, *1*(1), 43 (2016).
4. X. Wang, R. Yin, L. Zeng, M. Zhu, *Environ. Pollut.*, *253*, 100 (2019).

5. D. Mangla, A. Sharma, S. Ikram, *J. Hazard. Mater.*, *425*, 127946 (2022).

6. O. Baaloudj, I. Assadi, N. Nasrallah, A. El Jery, L. Khezami, A. A. Assadi, *J. Water. Process. Eng.*, *42*, 102089 (2021).

7. V. Homem, L. Santos, *J. Environ. Manage.*, *92*(10), 2304 (2011).

8. S. Zhang, Y. L. Yang, J. Lu, X. J. Zuo, X. L. Yang, H. L. Song, *J. Water Proc. Eng.*, *37*, 101421 (2020).

9. W. Yan, Y. Xiao, W. Yan, R. Ding, S. Wang, F. Zhao, *Chem. Eng. J.*, *358*, 1421 (2019).

10. Z. Z. Noor, Z. Rabiu, M. H. M. Sani, A. F. A. Samad, M. F. A., Kamaroddin, Perez, M. F., Z. A. Zakaria, *Curr. Pollut. Rep.*, 10, 1 (2021).

11. J. Overgaard, M. Overgaard, A. R. Timothy, *Br. J. Cancer.*, *48*(1): 27 (1983).

12. C. E. Voogd, J. J. Van der Stel, J. J. J. A. A. Jacobs, *Res-Fund. Mol. M.*, *26*(6), 483(1974).

13. W. Raether, H. Hänel, *Parasitol. Res.*, *90*: S19 (2003).

14. U. Guth,, W. Vonau, J. Zosel, *Meas. Sci. Technol.*, *20*(4), 042002 (2009).

15. B. J. Privett, J. H. Shin, M. H. Schoenfisch, *Anal. Chem.*, *82*(12): 4723 (2010).

16. J. Baranwal, B. Barse, G. Gatto, G. Broncova, A. Kumar, *Chemosensors*, *10*(9), 363 (2022).

17. G. Maduraiveeran, M. Sasidharan, V. Ganesan, *Biosens. Bioelectron.*, *103*, 113 (2018).

18. H. Mahmood Fashandi, R. Abbasi, A. Mousavi Khaneghah, *J. Food Process. Preserv.*, *42*(9), e13704 (2018).

19. M. B. Ahmed, J. L. Zhou, H. H. Ngo, W. Guo, *Sci. Total Environ. 532*, 112 (2015).

20. F. Yu, Y. Li, S. Han, J. Ma, *Chemosphere*, *153*, 365 (2016).

21. D. L. Strout, *J. Phy. Chem. A.*, *104*(15), 3364 (2000).

22. E. Shakerzadeh, *Physica E Low Dimens. Syst. Nanostruct. 78*, 1 (2016).

23. K. Kalateh, A. Abdolmanafi, *Int. J. New. Chem.*, *2*(1), 1 (2015).

24. M. R. Jalali Sarvestani, S. Abrahi Vahed, R. Ahmadi, *S. Afr. J. Chem. Eng.*, *47*, 60 (2024).

25. M. R. Jalali Sarvestani, M. Qomi, S. Arabi, *Nanomed. Res. J.*, *8*(4), 393 (2023).

26. M. R. Jalali Sarvestani, Z. Doroudi, *Russ. J. Phys. Chem. A.*, *97*(6), 1282 (2023).

27. M. R. Jalali Sarvestani, M. Gholizadeh Arashti, B. Mohasseb, *Int. J. New. Chem.*, *7*(2), 87 (2020).

28. M. R. Jalali Sarvestani, Z. Doroudi, *Russ. J. Phys. Chem. A.*, *95*(Suppl 2), S338 (2021)

29. M. R. Jalali Sarvestani, Z. Doroudi, R. Ahmadi, *Russ. J. Phys. Chem. B.*, *16*(1), 185 (2022).

30. J. Beheshtian, M. Kamfiroozi, Z. Bagheri, A. A. Peyghan, *Chinese. J. Chem. Phys.*, *25*(1), 60 (2012).

31. GaussView, Version 6.1, Roy Dennington, Todd A. Keith, and John M. Millam, Semichem Inc., Shawnee Mission, KS, (2016).

32. S. Melchor, J. A. Dobado, *J. Chem. Inf. Comput.,* 44, 1639 (2004).

33. Gaussian 16, Revision C.01, M. J. Frisch, G. W. Trucks, H. B. Schlegel, G. E. Scuseria, M. A. Robb, J. R. Cheeseman, G. Scalmani, V. Barone, G. A. Petersson, H. Nakatsuji, X. Li, M. Caricato, A. V. Marenich, J. Bloino, B. G. Janesko, R. Gomperts, B. Mennucci, H. P. Hratchian, J. V. Ortiz, A. F. Izmaylov, J. L. Sonnenberg, D. Williams-Young, F. Ding, F. Lipparini, F. Egidi, J. Goings, B. Peng, A. Petrone, T. Henderson, D. Ranasinghe, V. G. Zakrzewski, J. Gao, N. Rega, G. Zheng, W. Liang, M. Hada, M. Ehara, K. Toyota, R. Fukuda, J. Hasegawa, M. Ishida, T. Nakajima, Y. Honda, O. Kitao, H. Nakai, T. Vreven, K. Throssell, J. A. Montgomery, Jr., J. E. Peralta, F. Ogliaro, M. J. Bearpark, J. J. Heyd, E. N. Brothers, K. N. Kudin, V. N. Staroverov, T. A. Keith, R. Kobayashi, J. Normand, K. Raghavachari, A. P. Rendell, J. C. Burant, S. S. Iyengar, J. Tomasi, M. Cossi, J. M. Millam, M. Klene, C. Adamo, R. Cammi, J. W. Ochterski, R. L. Martin, K. Morokuma, O. Farkas, J. B. Foresman, and D. J. Fox, Gaussian, Inc., Wallingford CT, 2016.

34. N. M. O'Boyle, A. L. Tenderholt, K. M. Langner. *J. Comp. Chem.*, 29, 839 (2008).

35. AIM2000. *J. Comput. Chem.*, 22, 545 (2001).

36. M. Marianski, J. J. Dannenberg, *J. Phys. Chem. B.*, *116*(4), 1437 (2012).

37. O. P. Charkin, *Russ. J. Inorg. Chem.*, **68**, 430 (2023).

38. O. V. Mikhailov, D. V. Chachkov, *Russ. J. Inorg. Chem.*, **65**, 887 (2020).

39. R. Maizi, R. Ksouri, N. Cheghib, N. *et al. Russ. J. Inorg. Chem.* **68**, 1019 (2023).

40. D. V. Chachkov, O. V. Mikhailov, *Russ. J. Inorg. Chem.* **64**, 628 (2019).

41. A. M. Safiulina, N. E. Borisova, A. V. Lizunov, *Russ. J. Inorg. Chem.* **68**, 1650 (2023).

42. D. T. Nguyen Van Ha, Dat, N. H. Huy, *Russ. J. Inorg. Chem.* **67**, 2228 (2022).

43. B. Hassani, M. Karimian, N. Ghoreishi Amin, *Int. J. New. Chem.*, *11*(3), 204 (2024).

44. S. Tayebi-Moghaddam, M. Aliakbari, K. Tayeboun, *Int. J. New. Chem.*, *11*(2), 82 (2023).

45. M. Rezaei Sameti, M. Barandisheh Naghibi, *Int. J. New. Chem.*, *11*(1), 15 (2023).

46. Abrahi Vahed, S., & Hemmati Tirabadi, F., (2023). *Int. J. New. Chem.*, *10*(4), 288.

47. F. Mohammad Alipour, M. Babazadeh, E. Vessally, A. Hosseinian, P. Delir Kheirollahi Nezhad, *Int. J. New. Chem.*, *10*(3), 197 (2023).

48. R. Farahani, T. Madrakian, A. Afkhami, *Int. J. New. Chem.*, *9*(4): 383 (2023).

HOW TO CITE THIS ARTICLE

Pedram Niknam Rad, Fatemeh Ashtari Mahini, "**Boron Nitride Nanocluster ($B_{12}N_{12}$) Interaction with Nimorazole: A Comprehensive Theoretical Investigation**" International Journal of New Chemistry., 2024; 11(4), 424-442. DOI: 10.22034/ijnc.2024.713325